An Efficient Supervised Approach for Retinal Person Identification using Zernike Moments

Shubhra Aich
Samsung R&D Institute Bangladesh
Dhaka, Bangladesh

G M Al Mamun
Samsung R&D Institute Bangladesh
Dhaka, Bangladesh

ABSTRACT
Zernike moments map images using orthogonal basis functions. These moments have the advantages of rotation invariance, robustness and minimum information redundancy. In this paper, we focus on distinguishable pattern analysis of the retinal fundus images for person identification using Zernike moments. These moments are used to form 11-D feature vectors and k-nearest neighbor (kNN) classifier is used for person identification on publicly available DRIVE and STARE databases. This method outperforms all the existing methods with accuracy of 100% and 98.64% on DRIVE and STARE databases respectively. Its smaller dimension of feature vector, simplicity and robustness make this method suitable for real-time retinal person identification scheme.

General Terms – Biometrics, security, pattern recognition.

Keywords – Zernike moments, rotation invariance, retinal biometrics, kNN classifier, person identification.

1. INTRODUCTION
Biometrics refers to the automatic recognition and identification of individuals based on their physical (fingerprint, palmprint, hand geometry, vein, face, iris, retina, ear etc.) or behavioral (voice, signature, keystroke etc.) characteristics. For any measurement to be qualified as a biometric feature, it must have to possess the qualities like, universality, distinctiveness, permanence and collectability [1]. Having all the qualities mentioned above, retinal vessel pattern is not easy to replicate or forger and also it is free from the effects of the surroundings. Moreover, retinal vasculature rarely changes over the entire lifetime. Even, retinal vessel patterns are different between identical twins [2]. Despite all these effective characteristics of retinal vasculature as a biometric feature, it failed to gain much popularity over other biometrics in the past decades because of hardware limitations, i.e. high cost and lack of sophistication. However, with the drastic technological development in the past few years, retinal identification can now evolve as one of the most reliable biometric security systems of all time. Considering this fact, modeling of retinal pattern would be of high interest since effective and distinctive modeling of this pattern with fewer parameters would greatly simplify the implementation and processing of personal identification system using retinal fundus images and thus make this scheme a more reliable candidate as real-time biometric security system. In this paper, (1) prominent portions of the retinal vasculature are extracted; (2) 11-D distinguishable feature vector is formed using Zernike moments and (3) distinguishability of feature vectors are tested for the purpose of person identification using kNN classifier.

2. STATE OF THE ART
Some of the retinal authentication methods are based on minutiae features, i.e. ridge endings, bifurcations and cross points [3]-[6]. Pabitha and Latha [3] used bifurcation points template and noninvertible construction algorithm (NIC) to generate authentication template. Choras [4] used Gabor wavelet features along with minutiae based features. Barkhoda et al. [7] proposed angular and radial partitioning and 1-D Fourier transform for rotation invariant edge feature extraction. Farzin et al. [8] proposed polar transform on vessel extracted binary image for rotation invariance followed by multilevel wavelet decomposition and then pulse amplitude based feature extraction. Combination of 2-D Fourier and wavelet transform is used by Sabaghi et al. [9]. Due to varying thickness of retinal vasculature, multilevel energy distribution of wavelet can be used for feature analysis of the retinal authentication system. This technique is used by Shahnazi et al. [10] where wavelet energy feature (WEF) is proposed for person identification. Tabatabaee [11] proposed combination of central Fourier-Mellin transform (FMT) harmonics and complex moment magnitudes as feature vectors and Fuzzy C-means clustering for classification. Even, simple correlation and covariance matrix based recognition method also exists [12] for retinal identification.

Fig 1: RGB image of a retinal fundus.

3. PROPOSED METHOD
In this paper, a new supervised method is proposed for retinal person identification based on kNN classifier. The feature vector is computed using Zernike moments on the binary preprocessed version of the retinal fundus image. The method can be classified into the following steps: (1) field of view (FOV) extraction, (2) preprocessing for vessel enhancement, (3) extraction of prominent vasculature skeleton and (4) feature extraction using Zernike moments.

3.1 Field of View (FOV) Extraction

Since the RGB image of the retinal fundus looks reddish (Fig. 1), the red plane is brighter than the other two planes. Hence, it is convenient to separate the circular FOV region from the dark unwanted background of the image using red plane only.

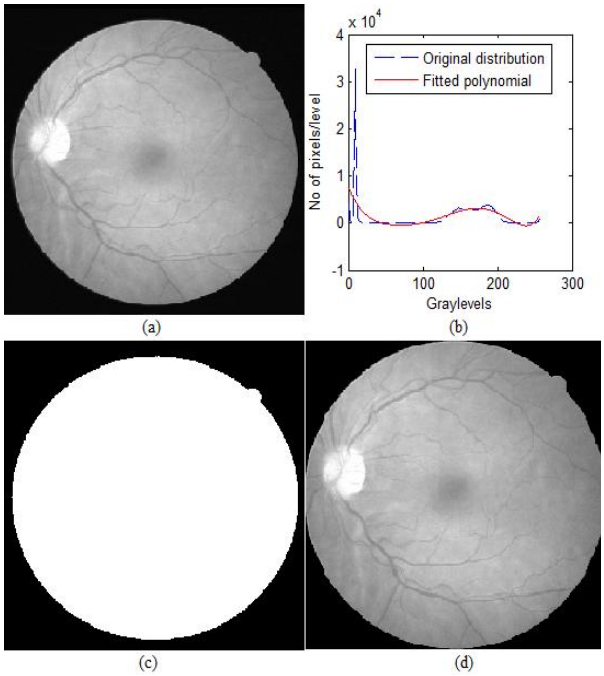

Fig 2: Illustration of the FOV extraction process: (a) Red plane of the original RGB image. (b) 2-D plot of the red plane histogram and fitted polynomial over the distribution. Original distribution of number of pixels is shown here using blue dashed line and the fitted polynomial is shown with solid red line. (c) FOV extracted using the determined threshold is shown as a circular white disc. (d) Red plane image in (a) reshaped according to the diameter of the FOV.

To do this, first histogram of the red plane is calculated in the range [0,255]. From the 2-D plot of the histogram, that is, taking the range of gray-levels [0,255] along the x-axis and the number of pixels per level along the y-axis, it is seen experimentally that, the dark unwanted region outside the FOV and the R-values (red plane values) of the RGB image of FOV form two clearly distinguishable clusters as shown in Fig. 2(b). To smooth the shape of the curve of this distribution, a polynomial is fitted over its frequency envelope. The polynomial is chosen to be of order six experimentally. The threshold for the separation in between the FOV region and the dark region outside FOV is thus selected as the lowest point in between these two clusters. All the planes, i.e. red, green and blue plane graylevel images are reshaped according to the diameter of the FOV (Fig. 2(d)).

3.2 Preprocessing for Vessel Enhancement

After extracting the circular FOV using the red plane of the RGB fundus image, the green plane is taken into account for further processing since this plane represents the retinal vasculature with better contrast than the other two planes [13]. It is even visually be well-understood from the RGB fundus image that the differentiable characteristics among retinal images of different persons lie greatly in their vessel tree structure. Hence, to extract differentiable features from fundus images, it is a prerequisite to enhance the image so that the prominent portions of the vasculature can easily be extracted by simple processing afterwards. Also, in retinal vessel detection methodologies, it is emphasized to classify the pixels as vessel or nonvessel with as much accuracy as possible and so this pixel classification task there is highly computation-costly. However, in case of retinal person identification, it is not essential to have the high level detail of the retinal vasculature. Rather, only the prominent portions of the vessel tree structure seem to be sufficient to differentiate among persons in the person identification scheme.

Taking all the above mentioned facts into account,

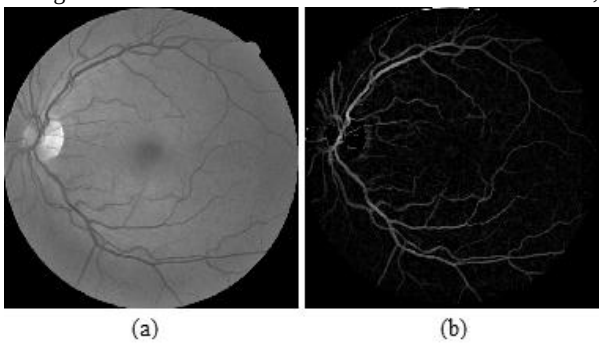

Fig 3: (a) FOV extracted green plane image. (b) Vessel enhanced image after preprocessing the image in (a).

preprocessing for vessel enhancement is performed according to Aquino et al. [14]. In [14], green plane is first filtered using opening operation by 3 pixel diameter disc to remove the vessel central light reflexes. Let us call this filtered image I_0. Next, to remove the nonvessel background intensity variation inside FOV, the output of the previous step (I_0) is filtered using a (3x3) mean filter to remove salt and pepper noise. Next level of smoothing is done by Aquino et al. [14] convolving the image with a (9x9) Gaussian kernel ($\mu = 0$, $\sigma = 1.8^2$). Then, background estimation (I_B) of the green plane image is formed by averaging the Gaussian convolved version of the image with mean kernel. In this paper, the size of the mean kernels chosen experimentally for DRIVE and STARE databases are (69x69) and (99x99) respectively. This variation in size is due to different image sizes in the two databases. Before averaging, Aquino et al. [14] filtered the dark region outside FOV with the mean value of the FOV pixels so that the dark region has no effect on the border of the circular FOV. Thus a difference matrix is created as follows:

$$D = I_0 - I_B \tag{1}$$

Converting the range of this difference matrix into [0, 255], the shade-corrected version (I_{SC}) of the original green plane image is created. For intensity adjustment, the homogenized image (I_H) is then constructed using the following formulae [14]:

$$I_H = \begin{cases} 0; & g < 0 \\ 255; & g > 255 \\ g; & otherwise \end{cases} \tag{2}$$

where

$$g = I_{SC} + 128 - I_{SC\_MAX} \tag{3}$$

Here, I_{SC_MAX} is the modal value of I_{SC}. Finally, the vessel enhanced image shown in Fig. 3(b), is constructed by Aquino

et al. [14] using the Top-Hat transformation on the complementary version of the homogenized image.

3.3 Extraction of Prominent Vasculature Skeleton

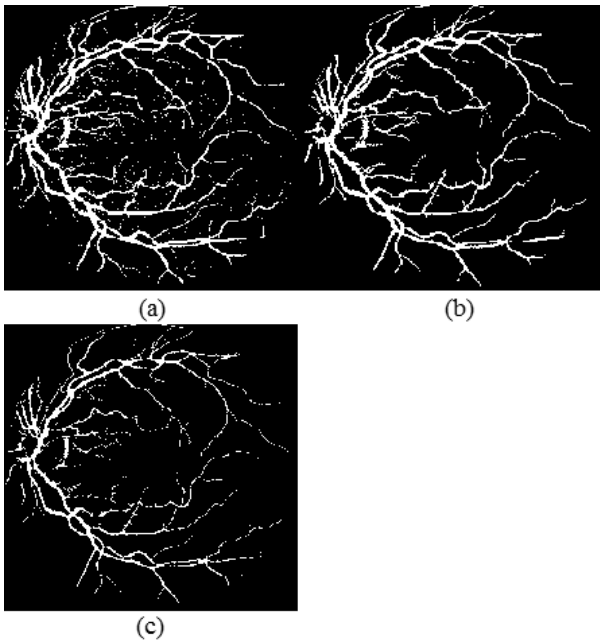

Fig 4: Illustration of the prominent vasculature skeleton extraction process: (a) Binary image derived from vessel enhanced image after global thresholding. (b) Image after salt and pepper noise and unwanted small blocks removal from binary image using object detector. (c) Prominent vasculature skeleton after morphological thinning.

Because the intensity adjustment is performed in the preprocessing stage, a global threshold can be used here to preserve the most parts of the prominent portions of the vessel tree structure. Here the global threshold value is selected experimentally to be 10. Also, all the pixel values outside the circular FOV region which has been extracted before are made forcefully the lowest value of the range that is zero here for the range [0, 255].

After Binarization, the binary image contains unwanted small blocks and salt and pepper noise along with prominent vessel tree structure. To remove these unwanted blocks and noise, the image is filtered using a binary object detector. This object detector identifies objects in a binary image using eight-connectivity and considers objects lower than certain area of pixels as noise and removes them. The threshold value of the area in between false object or noise and true object is chosen experimentally to be 30 pixels. Later, morphological thinning operation is performed on the image to bring out the skeleton of the prominent vasculature (Fig. 4(c)).

3.4 Feature Extraction Using Zernike Moments

Complex Zernike moment of order p is given by [15]

$$A_{pq} = \frac{p+1}{\pi} \iint dxdy\ f(x,y)\left[V_{pq}(\rho,\theta)\right]^{*} \qquad (4)$$

This is applicable for image function *f(x, y)* where x and y are both continuous, whereas for discrete x and y, the above formula for complex Zernike moment can be rewritten as [16]

$$A_{pq} = \frac{p+1}{\pi} \sum_{over\ unit\ circle} \sum f(x,y)\left[V_{pq}(\rho,\theta)\right]^{*} \qquad (5)$$

where p = 0, 1, 2, … ∞ and q takes on positive and negative integer values so that [15]

$$p - |q| \text{ is even and } |q| < p \qquad (6)$$

(ρ,θ) is the polar representation of (x, y) and $V_{pq}(\rho,\theta)$ is the Zernike polynomial given by [16]

$$V_{pq}(x,y) = V_{pq}(\rho,\theta) = R_{pq}(\rho)e^{iq\theta} \qquad (7)$$

where $R_{pq}(\rho)$ is the radial polynomial given by [16]

$$R_{pq}(\rho) = \sum_{s=0}^{\frac{p-q}{2}} (-1)^{s} \frac{(p-s)!}{s!\left(\frac{p+q}{2}-s\right)!\left(\frac{p-q}{2}-s\right)!} \rho^{p-2s} \qquad (8)$$

Zernike moments are computed over the unit circle, i.e. $x^2 + y^2 \leq 1$, where the center of the image is taken as the center of unit circle and so pixels outside the unit circle of the image are not considered for the computation [16].

As effects of translation have been cancelled by finding the FOV region and reshaping the image accordingly before, now it is necessary to find some techniques to extract rotation invariant features. Zernike moments serve this purpose very well with its rotation invariant property [16]

$$A_{pq}^{\phi} = A_{pq}\, e^{-iq\phi} \qquad (9)$$

where A_{pq}^{ϕ} is the p[th] order complex Zernike moment extracted from the ϕ radian rotated version of the original image function *f(x,y)*. From (9), it is clear that complex Zernike moments of an image function and its rotated version vary only in phase, not in magnitude. Hence, magnitudes of the complex Zernike moments can be used as rotation invariant features.

Moreover, higher order Zernike moments retrieve image function characteristics in greater detail than that of lower order moments. By definition of complex Zernike moments in (5) and (6), from 2[nd] order to 12[th] order, considering only positive integers of repetition q, 47 pairs of order p and repetition q are possible for which complex Zernike moments can be calculated. However, experimentally, only 11 of the 47 possible pairs are selected to calculate moments because moments calculated from these 11 pairs seem to show sufficient discrimination power in person identification phase. For even and odd orders, only repetition, that is, q, of values 2 and 3 are considered for moment calculation. The list of order and repetition pairs, that is, (p, q) pairs in (5), used to calculate moment features is shown in Table 1.

4. EXPERIMENTAL RESULTS

This method is evaluated on two publicly available DRIVE [17] and STARE [18] databases. The DRIVE and the STARE databases contain images of 40 and 20 different persons

respectively- one image per person. For identification test purpose, each image is rotated 5 times with rotation step of 5 degree in both clockwise and anticlockwise directions to generate a total of 11 images per person. Thus, in total 440 and 220 images exist in DRIVE and STARE databases respectively to test of the proposed method.

Table 1. Order-repetition pairs used for moment calculation

Order	2	3	4	5	6	7	8	9	10	11	12
Repetition	2	3	2	3	2	3	2	3	2	3	2

This method is tested on leave-one-out error estimation basis using k-nearest neighbor (kNN) classifier on the above mentioned extended DRIVE and STARE databases. For DRIVE database, identification accuracy of 100% is obtained. For STARE database, an identification accuracy of 98.64% with 3 false identifications in 220 images is obtained. A comparison to the best recent methodologies on the basis of accuracy is listed in Table 2 below.

5. DISCUSSION AND FUTURE WORK

In this paper, an efficient identification scheme is proposed based on retinal fundus images using only 11-D feature vectors through the incorporation of Zernike moments. It is demonstrated that only 11 parameters are sufficient to identify individuals in a retinal identification system. Hence, this method can be considered to be one of the candidates for faster and simpler real-time biometric security system implementation using retinal images. The proposed method is evaluated on two popular standard databases – DRIVE and STARE. The identification accuracy of this method is 100% for DRIVE database which contains few mildly affected fundus images. However, accuracy falls to 98.64% for STARE database because most of the images of this database are affected. Therefore, further improvement of recognition accuracy for affected images will appear as a challenge in future studies.

Table 2. Comparison of different methods based on identification accuracy

Methods	Accuracy (%)		
	DRIVE	STARE	VARIA
Farzin et al. [8]	99.00	-	-
Barkhoda et al.[7]	99.75	-	-
Sabaghi et al. [9]	99.10	-	-
Pabitha and Latha [3]	100.00	90.10	96.30
Aich (this work)	**100.00**	**98.64**	**-**

6. ACKNOWLEDGMENT

This work was supported by **Samsung R&D Institute Bangladesh (SRBD)** which is a direct subsidiary of **Samsung Electronics**, a concern of **Samsung Group**, the largest conglomerate in the world.

7. REFERENCES

[1] A. K. Jain, A. Ross and S. Prabhakar, "An introduction to biometric recognition," *IEEE Trans. Circuits Syst. Video Techn*., vol. 14, no. 1, pp 4-20, Jan 2004.

[2] P. Tower, "The fundus oculi in monozygotic twins: report of six pairs of identical twins," *Archives of Ophthalmology,*vol. 54, no. 2, pp 225-239, 1955 .

[3] M. Pabitha and L. Latha, "Efficient approach for retinal biometric template security and person authentication using noninvertible constructions," *Int, J. Computer Applications*, vol. 69, no. 4, pp 28-34, May 2013.

[4] R. S. Choras, "Retina recognition for biometrics," *ICIDM*, Langkawi, Malaysia, 2012, pp 177-180.

[5] M. U. Akram, A. Tariq and S. A. Khan, "Retinal recognition: Personal identification using blood vessels," *ICITST*, Abu Dhabi, UAE, 2011, pp 180-184.

[6] S. Qamber, Z. Waheed and M. U. Akram, "Person identification system based on vascular pattern of human retina," *CIBEC*, Cairo, Egypt, 2012, pp 64-67.

[7] W. Barkhoda, F. Akhlaqian, M. D. Amiri and M. S. Nouroozzadeh, "Retina identification based on the pattern of blood vessels using fuzzy logic," *EURASIP J. Adv. Sig. Proc.2011:113(2011).*

[8] H. Farzin, H. Abrishami-Moghaddam and M. S. Moin, "A novel retinal identification system," Hindawi Publ. Corp., *EURASIP J. Adv. Sig. Proc.*, vol. 2008.

[9] M. Sabaghi, S. R. Hadianamrei, M. Fattahi and M. R. Kouchaki and A. Zahedi, "Retinal identification system based on the combination of Fourier and Wavelet transform," *J. Sig. Info. Proc.*, pp 35-38, 2012.

[10] M. Shahnazi, M. Pahlevanzadeh and M. Vafadoost, "Wavelet based retinal recognition," *ISSPA*, Sharjah, UAE, 2007, pp 1-4.

[11] H. Tabatabaee, A. M. Fard and H. Jafiriani, "A novel human identifier system using retina image and fuzzy clustering," *ICTTA*, Damascus, Syria, 2006, pp 1031-1036.

[12] S. N. Kakarwal and R. R. Deshmukh, "Analysis of retina recognition by correlation and covariance matrix," *ICETET*, Goa, India, 2010, pp 496-499.

[13] T. Walter, P. Massin, A. Erginay, R. Ordonez, C. Jeulin and J. C. Klein, "Automatic detection of microaneurysms in color fundus images," *Med. Imag. Anal.*, vol. 11, pp 555-566, 2007.

[14] D. Marin, A. Aquino, M. E. Gegundez-Arias and J. M. Bravo, "A new supervised method for blood vessel segmentation in retinal images by using gray-level and moment invariants-based features," *IEEE Trans. Med. Imag.*, vol. 30, no. 1, pp 146-158, Jan 2011.

[15] M. R. Teague, "Image analysis via the general theory of moments," *J. Opt. Soc. Am.*, vol. 70, no. 8, pp 920-930, Aug 1980.

[16] A. Khotanzad and Y. H. Hong, "Rotation invariant pattern recognition using Zernike moments," *ICPR*, Cambridge, UK, 1988, pp 326-328.

[17] DRIVE database [online]. Available: http://www.isi.uu.nl/Research/Databases/DRIVE/

[18] STARE database [online]. Available: http://www.parl.clemson.edu/~ahoover/stare/index.html